

Quantum chemical study of the electronic properties of an Iridium-based photosensitizer bound to medium-sized silver clusters

Olga S. Bokareva* and Oliver Kühn
*Institut für Physik, Universität Rostock,
 Universitätsplatz 3, D-18055 Rostock, Germany*

(Dated: January 20, 2015)

The equilibrium structures and electronic excitation spectra of the Ir(III) photosensitizer $[\text{Ir}(\text{ppy})_2(\text{bpy})]^+$ bound to medium-sized silver clusters Ag_n ($n=19, 20$) are investigated using time-dependent density functional theory. The long-range corrected LC-BLYP approach is used with a system-specific range separation parameter. The weak physisorption of the hybrid complexes yield only small changes in the broadened absorption spectra of the hybrid system as compared with its constituents. However, the density of states as well as the fine structure of the spectra is strongly modified upon complexation. It is shown that the standard range separation parameter (0.47 bohr^{-1}) cannot predict these properties correctly and the optimized value of 0.16 bohr^{-1} should be used instead.

I. INTRODUCTION

The combination of metal nanoparticles or nanowires with various organic adsorbates such as dyes, peptides, and J-aggregates is an active area of research with applications in bio-sensing, catalysis, and medicine [1–5]. Numerous theoretical and experimental studies of nanoparticle-organic hybrid systems have been reported (for reviews, see, e.g., Refs. [6–9]). These hybrid systems exhibits new composition dependent properties, which differ from those of the separate constituents. This includes the enhancement or quenching of fluorescence, absorption, and Raman scattering due to surface and plasmon resonances, the broadening of the absorption range to yield an antenna effect, and modified “redox” properties; see, e.g., Refs. [10–14].

In the present communication we discuss results on the electronic properties of a model system comprised of the $[\text{Ir}(\text{ppy})_2(\text{bpy})]^+$ photosensitizer (IrPS) shown in Fig. 1, bound to medium-sized silver clusters Ag_n ($n=19, 20$). Our choice of the system is motivated by the use of heteroleptic Ir(III) complexes as photosensitizers in a photocatalytic system for water splitting introduced by Beller et al. [15]. The original homogeneous system includes triethylamine as a sacrificial reductant and a series of iron carbonyls as water reduction catalysts. The absorption spectrum of the IrPS overlaps with the sun’s spectrum only in its long wave length tail between 300 and 450 nm [16]. Therefore, extending the range of absorption further into the visible by coupling the IrPS to silver nanoparticles might provide a means to enhance the overall efficiency of this photocatalytic system.

Because of size of the systems under study, density functional theory (DFT) [17] and its extension into the time-dependent (TD) domain in the linear response limit [18] is the natural choice for studying ground and ex-

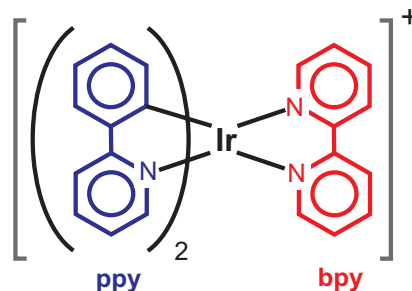


Figure 1: Chemical formula of the photosensitizer $[\text{Ir}(\text{ppy})_2(\text{bpy})]^+$ (IrPS).

cited state properties. However, the correct description of long-range charge-transfer (CT) properties, which is of mandatory for hybrid systems, can not be achieved applying conventional DFT functionals [19–23]. By introducing exact Hartree-Fock exchange in long-ranges corrected schemes as LC-BLYP [24–26] or CAM-B3LYP [27], the correct asymptotic behavior and more balanced description for CT states is obtained. In our previous study on bare IrPS [16], the LC-BLYP approach was shown to give excitation energies in good agreement with experimental data and results of CASSCF/CASPT2 calculations.

The binding of IrPS to small model silver clusters (one to six silver atoms) has been studied using the LC-BLYP approach in Ref. [28]. Already for this size of the hybrid system pronounced changes in the electronic absorption spectrum had been observed. Moreover, the electronic properties were found to be rather sensitive to the number of silver atoms, Binding energies and localization of HOMO and LUMO orbitals are found to oscillate with the number of silver atoms in an even/odd like fashion. Whether such a behavior propagates to larger clusters and how it influences the photophysical properties is the topic of the present study.

The paper is organized as follows. In Sec. II we give the computational details putting emphasis on the tuning of

*Electronic address: olga.bokareva@uni-rostock.de

the range-separation functional in LC-BLYP. The results are presented in Sec. III, including electronic ground state structures and electronic absorption spectra. A summary is provided in Sec. IV.

II. COMPUTATIONAL DETAILS

In the long-range separation approach LC-BLYP a parameter ω is introduced, which defines the separation of the Coulomb operator into long-range and short-range parts, with the long-range part then being described by the exact exchange integral. In a number of publications, it was demonstrated that an appropriate tuning of ω leads to a significant improvement of fundamental and optical gaps, CT and Rydberg excitation energies as well as ionization potentials (IPs) [29–32]. A systematic procedure for the determination of an optimal ω has been suggested in Refs. [33–35]. It is based on finding that ω , which minimizes the following functional

$$\begin{aligned} J(\omega) &= J_N(\omega) + J_{N+1}(\omega) \\ &= |\varepsilon_{\text{HOMO}}^\omega(N) + \text{IP}^\omega(N)| \\ &\quad + |\varepsilon_{\text{HOMO}}^\omega(N+1) + \text{IP}^\omega(N+1)|. \end{aligned} \quad (1)$$

In other words, the optimized ω will provide a compromise for fulfilling Koopmans' theorem simultaneously for systems with N (cation complex) and $N+1$ (neutral complex) electrons. In Eq. (1), $\varepsilon_{\text{HOMO}}^\omega$ and IP^ω is the HOMO energy and the IP, respectively.

In Ref. [36] we have studied the present systems and obtained optimized range-separation parameters for the bare IrPS, silver clusters Ag_n , and hybrid systems $\text{IrPS}-\text{Ag}_n$ ($n = 2, 10, 20$). Here, we give a more detailed account on the case of $\text{IrPS}-\text{Ag}_{10}$. In short, the IPs and HOMO energies of neutral species, anions, and cations have been obtained from single-point energy calculations at the optimized geometry of the electronic ground state. Similar to the small systems [28], the geometry optimization was carried out without symmetry constraints. Initial geometries of IrPS for further optimization were taken from Ref. [16] (assuming C_2 point symmetry [37]). The initial structures of Ag_{10} were taken from Ref. [38], those of Ag_{19} and Ag_{20} from Ref. [39], except tetrahedral Ag_{20} which had been studied before in Refs. [40–42]. Binding energies have been obtained including the counterpoise method to correct for the basis set superposition error (BSSE) [43, 44].

Vertical excitation spectra have been calculated by means of the TDDFT approach. The number of included transitions has been 450 and 650 for XXa and IXXo, respectively. A Lorentzian broadening (0.4 eV) has been added to the stick-spectra. Spin-forbidden transitions were not included in the present TDDFT investigation although they could have notable intensity due to the high spin-orbit coupling constant of Ir. All calculations were performed with the Gaussian09 program package

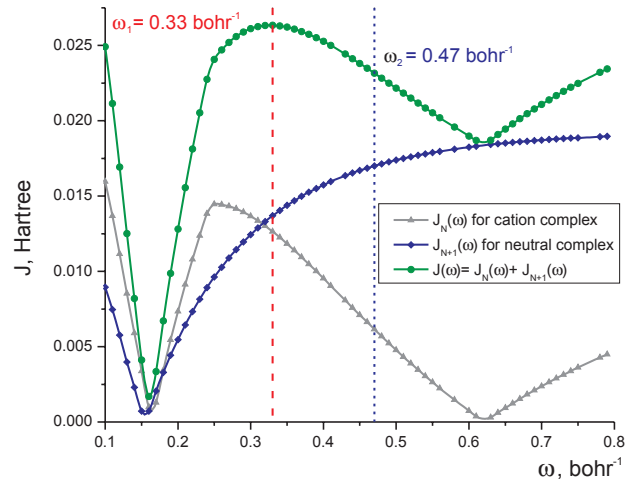


Figure 2: Optimization of range-separation parameter for the case of $\text{IrPS}-\text{Ag}_{10}$. The functions $J_N(\omega)$ and $J_{N+1}(\omega)$ are defined in Eq. (1) and represent the conditions for fulfilling Koopmans' theorem for the cationic and neutral species, respectively.

[45] using the LANL2DZ effective core potential basis set for Ir and Ag and the 6-31G(d) basis for all other atoms.

III. RESULTS AND DISCUSSION

A. Range-separation Parameter Optimization

In Fig. 2, the procedure for tuning ω is demonstrated for the case of $\text{IrPS}-\text{Ag}_{10}$. A minimum of $J(\omega)$ at 0.16 bohr^{-1} was found. Around 0.63 bohr^{-1} an additional higher energetic minimum occurs. This can be traced to the change of the character of the lowest adiabatic state of the cationic species, where the order of HOMO and HOMO-1 orbitals are interchanged. Here, the unpaired electron initially localized on the $\pi^*(\text{bpy})$ orbital of the reduced doublet IrPS is transferred to the $\sigma(\text{Ag}_{10})$ orbital [46].

The obtained optimal ω value is substantially smaller than values of 0.33 bohr^{-1} and 0.47 bohr^{-1} (shown as vertical lines in Fig. 2) implemented in common quantum chemical packages. This is not surprising since these (standard) values were determined for test sets of diatomics and small molecules [25, 47].

Since the inverse of ω reflects a characteristic distance for switching between short- and long-range parts of the exchange contribution, optimal ω values were shown to decrease with increasing system size and conjugation length [29, 30, 32, 35, 48–50]. This size-dependence, however, is not monotonous and there is a strong dependence on the electronic structure [32]. Optimal values of ω near 0.2 bohr^{-1} have been reported for various systems with characteristic electronic radii comparable to the present

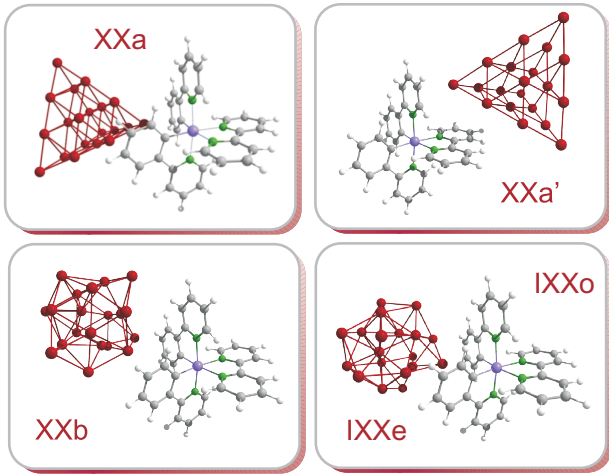


Figure 3: Optimized structures of IrPS–Ag₁₉ and IrPS–Ag₂₀ studied in this paper. The conformers labeled IXXe and IXXo are not distinguishable at the scale of the image.

ones, e.g., 0.214 bohr^{-1} was found for pentacene-C₆₀ [51]; for other examples see Refs. [32, 35, 48].

As shown in Ref. [36] there is only a slight variation of ω when going from IrPS, via Ag_{*n*} ($n = 10, 20$) to IrPS–Ag_{10, 20}. Thus, in the following we provide results on excited states obtained using $\omega = 0.16 \text{ bohr}^{-1}$ for all compounds. It turned out the ground state geometries of the present systems are little affected by the choice of ω . The corresponding tests have been performed for IrPS, Ag₂, IrPS–Ag₂, and IrPS–Ag₁₉. Therefore, we have used the standard $\omega_2 = 0.47 \text{ bohr}^{-1}$ for the ground state optimization. Selected TDDFT calculations are also performed with the latter value in order to study the influence of ω on the absorption spectrum.

B. Ground electronic state

In our previous study of IrPS bound to small ($n \leq 6$) silver clusters [28], we found that configurations in which Ag_{*n*} is situated in the cavities between ligands are the lowest in energy. Note that in all cases the interactions are “weak” and no chemical bonds are formed. Here, we extended our investigation to IrPS–Ag_{*n*} geometries with 19 and 20 silver atoms, however, focussing mostly on those structures where the cluster is located in the “ppy-ppy” cavity as shown in Fig. 3.

The differences in geometry of IrPS upon complexation with a silver cluster are only minor (maximal changes are 0.09 \AA and 4.6°); for an overview of geometries see Table I. The binding energies of the studied systems are in the range $1.5 - 2.5 \text{ kJ/mol}$, which is about 10 times smaller than that of silver atoms in large nanoparticles [52] and smaller than in analogous systems with $n = 1 - 6$. This confirms the trend of a decrease of binding energies with the increase of cluster size found previously [28]. Such

a behavior can be explained by the fact that no stable complexes are formed, i.e. the interaction belongs to physisorption case and might be considered as a weak attraction between the ligands of IrPS and nearest atoms of silver cluster. The total binding energies (not divided by number of silver atoms) are $30\text{--}100 \text{ kJ/mol}$ for all systems disregarding the cluster size. Accounting for the BSSE decreases the binding energy by factor of about two for all cases. The change of ω from the standard to the optimized value has no uniform impact on binding energies. Changes of a factor of about two in both directions were observed. Note that the order of stability is sensitive to the value of range-separation parameter used. For clarity, we provide here only results of calculations with the optimal ω value. For the series of XX structures, the XXa conformer is the lowest in energy, while XXa’ and XXb are by 30.0 and 4.1 kJ/mol higher, respectively. For the IXX species, IXXe is more stable ($\Delta E = 38.2 \text{ kJ/mol}$). Nevertheless, in the following we also discuss the IXXo structure because of its unique electronic structure in the ground electronic state.

The representative frontier orbitals (LC-BLYP, $\omega = 0.16 \text{ bohr}^{-1}$) are given in Fig. 4 for the cases of IXXo and XXa. If the standard value of ω is applied then the HOMO-LUMO gap increases by about 1 eV for all cases. The shift is mainly due to the LUMO orbitals while the nature and order of orbitals remains the same.

The orbital structure differs for systems containing odd and even number of silver atoms. For an even number, the HOMO orbital is localized on the silver fragment (σ_{Ag}) and the LUMO is of $\pi_1^*(\text{bpy})$ type. For an odd number of silver atoms this situation is reversed: the unpaired electron is situated on the $\pi_1^*(\text{bpy})$ orbital as in the reduced IrPS, while the LUMO is localized on the silver fragment. A similar situation with one exception for IrPS–Ag₅ was found for smaller clusters [28] as well as for the much larger cluster IrPS–Ag₉₂ [53].

For 19 atoms two cases were found which slightly differ in geometry: IXXo (“o” means “odd”) follows the orbital rules just given and IXXe (“e” stands for “even”) is an exception where the unpaired electron is localized on the silver fragment. The “odd” and “even” groups can be also seen from the comparison of geometries, see Table I; the distances Ir–N_{bpy} and $r(\text{C–C})_{\text{bpy}}$ are shorter for the “odd” group and the IrPS in its reduced form (IrPS⁰).

C. Absorption spectra

The absorption spectra of IXXo and XXa are presented in Fig. 5. The standard (0.47 bohr^{-1}) and optimized ω values were applied for comparison. Because of the number of states considered and of the complex character of most states, we distinguish only between two types of orbitals: those localized on silver or on dye fragments, but do not consider the particular character of orbitals, e.g., $\pi(\text{ppy})$, $\pi(\text{bpy})$, or $d(\text{Ir})$ for IrPS. For each state different contributions have been summed up and the

Table I: Selected equilibrium geometric parameters of all $\text{IrPS} \cdots \text{Ag}_n$ compared to IrPS [16] and IrPS^0 [46] in the ground electronic states. For notation of structures see Fig. 3. Bond lengths in Å, angles in degrees.

Parameter ^a	IrPS	IrPS^0	IXXo	IXXe	XXa	XXa'	XXb
$r(\text{Ir}-\text{C}_{\text{ppy}})$	2.007	2.010	2.019	2.005	2.007	2.001	2.002
$r(\text{Ir}-\text{N}_{\text{ppy}})$	2.055	2.051	2.051	2.059	2.058	2.056	2.057
$r(\text{Ir}-\text{N}_{\text{bpy}})$	2.163	2.134	2.116	2.158	2.158	2.160	2.162
$r(\text{C}-\text{C})_{\text{ppy}}$	1.463	2.464	1.470	1.463	1.466	1.457	1.461
$r(\text{C}-\text{C})_{\text{bpy}}$	1.485	2.409	1.408	1.482	1.485	1.481	1.482
$r(\text{Ir}-\text{Ag})^{\text{b}}$	—	—	3.563	3.919	4.042	5.101	5.108
$\angle \text{ClrC}$	89.3	89.1	93.9	92.9	90.7	89.8	90.4
$\angle \text{N}_{\text{ppy}}\text{IrN}_{\text{ppy}}$	172.1	174.5	174.8	171.8	171.8	172.8	172.2
$d\text{ClrCN}$	92.4	96.1	95.8	93.2	93.3	95.0	94.6

^a For parameters including ppy, only those ppy fragment that is closer to the silver cluster is regarded. The parameters of second ppy fragment differ by no more than 0.04 ; ^b Distance between Ir and closest silver atom.

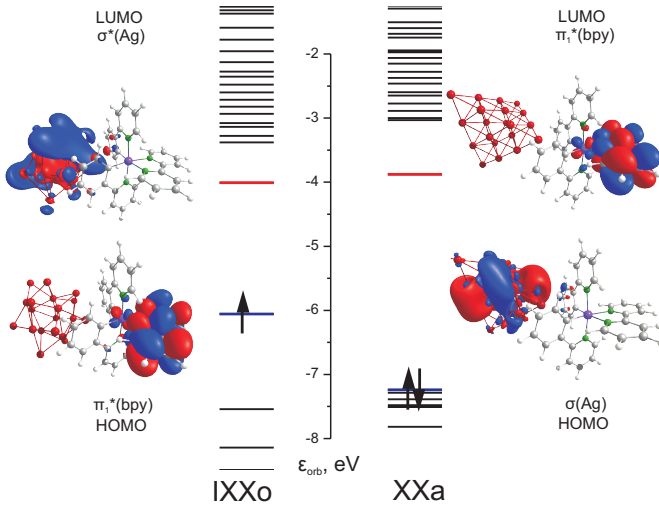


Figure 4: Molecular orbital energies and frontier orbitals for IXXo and XXa systems.

corresponding dominating character has been assigned. Most of transitions have very complex assignment and are marked as “mixed”. In Fig. 5 the spectra are shown as sticks and with a Lorentzian broadening.

All spectra have a clear maximum composed mainly by silver-localized transitions, which, for pure cluster spectra, would be called “plasmonic” excitations (collective excitation of electrons). Similar to the cases of small silver clusters [28], the hybrid systems support a new type of long-range intermolecular CT, corresponding to $\text{IrPS} \rightarrow \text{Ag}_n$ or $\text{Ag}_n \rightarrow \text{IrPS}$. These intermolecular CT transitions (denoted as IM to emphasize the their long-range nature) are marked with red bars in Fig. 5. The IM transitions have very different intensities, from almost zero to that comparable with silver plasmon-like transitions. Many transitions can not be attributed to pure IM type. but have a notable contribution of intramolecular CT character. These mixed transitions are marked with black bars in Fig. 5. In the lower panel of Fig. 5, electron density difference plots for transitions of IM and cluster localized types are given.

Comparing the spectra of XXa and IXXo with different

ω values, three important points should be highlighted. First, their maxima are shifted to the red by 0.4 eV for XXa and by 0.1 eV for IXXo. The positions of particular bands can hardly be compared as the assignment is very complex. Second, the density of states for the optimized ω is almost twice higher than for the standard ω . Finally, the distribution of oscillator strength depends on ω as well. This is particularly visible for the XXa system, where the optimized ω yields a double peak spectrum, which is in contrast to IXXo. For the standard ω XXa and IXXo have essentially the same line shape.

The changes of absorption spectra upon complexation are of general importance for possible photochemical and photophysical applications. Because of complicated assignment of single bands, the direct comparison of particular transitions is hindered and only the overall shapes can be compared. In Fig. 6 the broadened spectra for IXXo and XXa are compared to those of the pure constituents. For IXXo, we provide the spectra of reduced IrPS^0 and Ag_{19}^+ according to the ground electronic state structure, whereas for XXa the results for IrPS and Ag_{20} are given.

The broadening parameter was chosen in such a way as to reproduce the approximate width of experimental plasmonic band for silver clusters, which is about 50 nm [54, 55]. However, different types of transitions (local and CT), even in case of pure IrPS, could have a different broadening, which is not considered due to the lack of detailed information. For the case of smeared fine structures of spectra, we expect our results to be only slightly dependent on the variation of line shape and small changes in line widths of transitions of particular types. When discussing the changes in the broadened spectra in the following, one should keep in mind that the individual transitions and thus the unresolved fine structure of the spectrum is strongly modified upon complexation.

If we compare the absorption spectra of the hybrid systems with those of their constituents the following observations can be made: The maximum of the plasmonic band in the spectrum of IXXo is shifted by 0.2 eV to the blue and its width increases slightly. For XXa the maximum remains almost at the same position upon

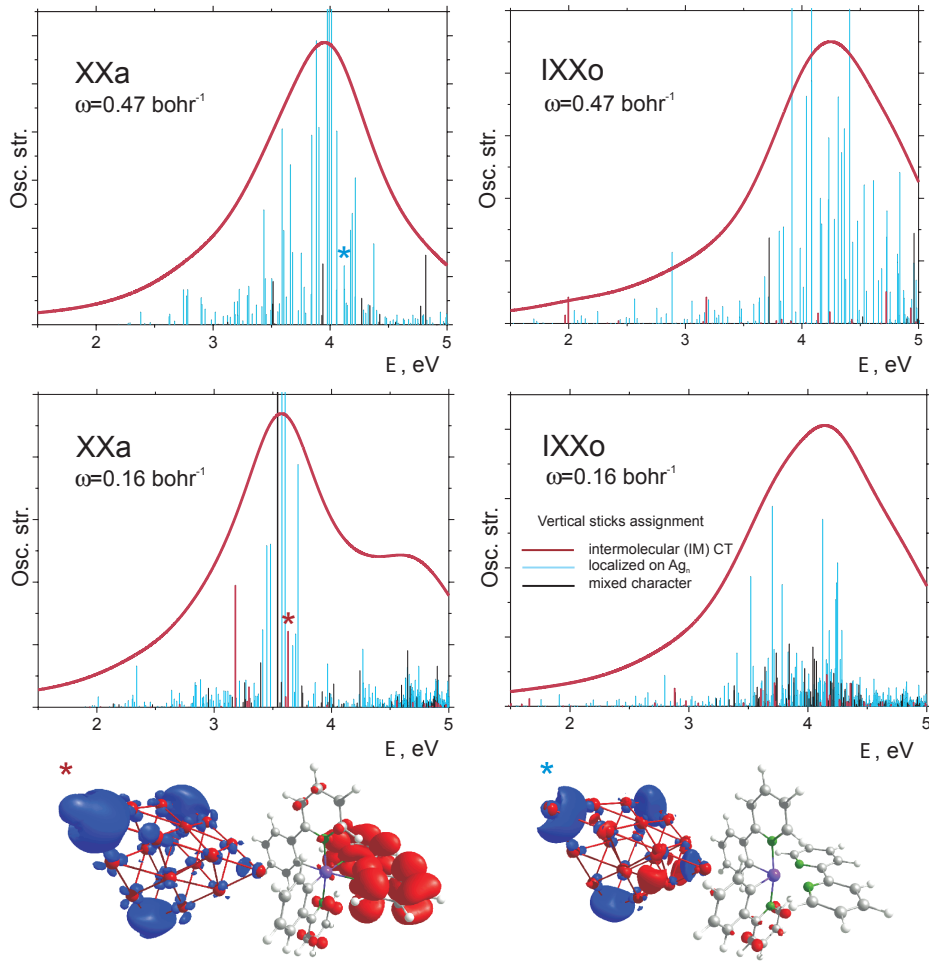


Figure 5: Upper panel: Selected vertical electronic singlet-singlet (for XXa) and doublet-doublet (for IXXo) TDDFT spectra calculated with LC-BLYP with standard and optimized ω parameter. Associated spectra are broadened with Lorentzians of width 0.4 eV. Lower panel: Electron density differences (contour value 0.0008) for selected transitions, which are marked with asterisks in upper panel. Red and blue colours correspond to particle and hole densities, respectively.

complexation with IrPS. The position and shape of this broad band is very similar for unbound and bound clusters. Some additional features in the spectra of XXa in the region from 4.5 to 5 eV could be attributed to the influence of IrPS through the manifold of new states with non-negligible IM CT character.

Figure 6 also contains the sum of spectra of the isolated dye and the cluster. It almost does not differ from the spectrum of the interacting hybrid system for XXa, and it is shifted only by about 0.2 eV to the blue for IXXo. But the density of states increases and most transitions have at least an admixture of IM character. Therefore, the spectra of hybrid systems cannot be considered as

perturbed spectra of metal clusters. Consequently, the photodynamics of the hybrid systems might strongly differ from those of pure IrPS.

IV. CONCLUSIONS

The interaction of an Ir(III)-based photosensitizer with silver clusters containing 19 or 20 atoms has been studied by means of TDDFT with a properly chosen range-separation parameter in the LC-BLYP functional. Although the interaction between dye and metal particle belongs to the case of weak physisorption, the properties

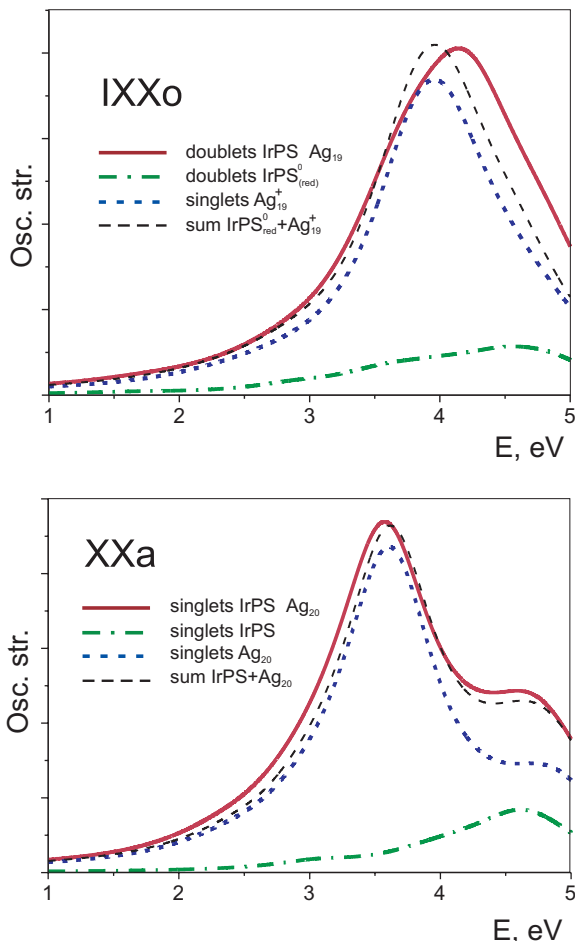


Figure 6: Calculated (LC-BLYP, $\omega = 0.16 \text{ bohr}^{-1}$) absorption spectra of pure IrPS, Ag_n , their sum, and combined systems IrPS-Ag_n ($n = 19, 20$). The width of the Lorentzian broadening has been 0.4 eV . Note that for IXXo the reduced IrPS and the oxidised Ag_{19} have been used as reference, in accord with the ground state orbital structure of this system.

of the hybrid systems differ notably from those of its constituents. This concerns the appearance of long-range intermolecular CT states, which might lead to a completely different photophysical and photochemical behaviour, including long-lived charge separation favourable for further reactions. The low resolution electronic excitation spectra are close to the sum of the spectra of the non-interacting constituents. However, the underlying den-

sity of electronic states and thus the fine structure of the spectra is strongly modified in the hybrid system, with the details depending on the number of silver atoms. The changes in the adsorption spectrum upon forming the hybrid system are mostly observed the region from 3 to 4.5 eV , but they are masked by the broad plasmonic type absorption band of the cluster.

If we extrapolate the obtained theoretical results to experimental observations the following considerations should be taken into account. First, metal clusters used for spectroscopic and catalytic studies are produced either chemically by reduction in solutions [56, 57] or with laser techniques, e.g., cluster beam generation utilizing arc discharge, magnetron sputtering, or laser vaporization (for review see, e.g., Ref. [58]). The resulting clusters are substantially larger compared to those used in our theoretical model and have a certain size distributions. Second, the clusters are produced either in solution or deposited on a plate. The deposited nanoclusters have the advantage of being protected from fast aggregation and thus are often applied in spectroscopic studies and also in catalysis providing more stable and long-living catalysts. The experimental maximum of plasmonic band for silver particles is in the range $375\text{--}430 \text{ nm}$ for an average diameter from 2 to 50 nm [54–57, 59] and produced in aqueous solution or embedded in solid substrate (SiO_2 , Cr_2O_3 , and MgF_2). The maximum of this peak shifts to the red with increasing the average cluster size and with increasing the dielectric constant of the surrounding medium. Consequently, the spectra of IrPS bound to silver clusters relevant in those experiments should be averaged over different cluster sizes and red-shifted as compared to those shown in Fig. 6. It can be expected that the differences between odd and even number of atoms in cluster will not be seen in this case. Further, the interaction between the silver clusters and the IrPS will be weakened due to the increase of the spectral separation. The consequences for the properties of the hybrid system still need to be explored.

Acknowledgments

This work has been supported by the European Union (European Social Funds, ESF) within the project "PS4H" and by the Ministry for education, science and culture of Mecklenburg-Vorpommern.

[1] J. Yu, S. A. Patel, and R. M. Dickson, *Angew. Chem. Int. Ed.* **46**, 2028 (2007).
 [2] S.-I. Tanaka, J. Miyazaki, D. K. Tiwari, T. Jin, and Y. Inouye, *Angew. Chem. Int. Ed.* **50**, 431 (2011).
 [3] K. E. Sapsford, J. Granek, J. R. Deschamps, K. Boeneman, J. B. Blanco-Canosa, P. E. Dawson, K. Susumu, M. H. Stewart, and I. L. Medintz, *ACS Nano* **5**, 2687

(2011).
 [4] S. Halivni, A. Sitt, I. Hadar, and U. Banin, *ACS Nano* **6**, 2758 (2012).
 [5] R. Tel-Vered, O. Yehezkeli, and I. Willner, *Adv. Exp. Med. Biol.* **733**, 1 (2012).
 [6] E. Dulkeith, A. Morteau, T. Niedereichholz, T. Klar, J. Feldmann, S. Levi, F. van Veggel, D. Reinhoudt,

- M. Möller, and D. Gittins, Phys. Rev. Lett. **89**, 203002 (2002).
- [7] P. Anger, P. Bharadwaj, and L. Novotny, Phys. Rev. Lett. **96**, 113002 (2006).
- [8] V. Pustovit and T. Shahbazyan, Phys. Rev. B **83**, 085427 (2011).
- [9] G. Zweigle and J. McHale, J. Phys. Chem. C **115**, 13693 (2011).
- [10] W. Wenseleers, F. Stellacci, T. Meyer-Friedrichsen, T. Mangel, C. A. Bauer, S. J. K. Pond, S. R. Marder, and J. W. Perry, J. Phys. Chem. B **106**, 6853 (2002).
- [11] J. Lee, A. O. Govorov, and N. A. Kotov, Nano Letters **5**, 2063 (2005).
- [12] S. Saini, S. Bhowmick, V. B. Shenoy, and B. Bagchi, J. Photochem. Photobiol. A **190**, 335 (2007).
- [13] W. Zou, C. Visser, J. A. Maduro, M. S. Pshenichnikov, and J. C. Hummelen, Nature Photonics **6**, 560 (2012).
- [14] V. N. Rai, A. K. Srivastava, C. Mukherjee, and S. K. Deb, Applied Optics **51**, 2606 (2012).
- [15] F. Gärtner, B. Sundararaju, A.-E. Surkus, A. Boddien, B. Loges, H. Junge, P. H. Dixneuf, and M. Beller, Angew. Chem. Int. Ed. **48**, 9962 (2009).
- [16] S. I. Bokarev, O. S. Bokareva, and O. Kühn, J. Chem. Phys. **136**, 214305 (2012).
- [17] W. Koch and M. C. Holthausen, *A Chemist's Guide to Density Functional Theory, 2nd Edition* (2001), Wiley ed.
- [18] M. E. Casida, vol. 1 of *Recent Advances in Computational Chemistry* (World Scientific, 1995).
- [19] A. Dreuw, J. L. Weisman, and M. Head-Gordon, J. Chem. Phys. **119**, 2943 (2003).
- [20] A. Dreuw and M. Head-Gordon, Chem. Rev. **105**, 4009 (2005).
- [21] M. J. G. Peach, P. Benfield, T. Helgaker, and D. J. Tozer, J. Chem. Phys. **128**, 044118 (2008).
- [22] R. Richard and J. Herbert, J. Chem. Theor. Comp. **7**, 1296 (2011).
- [23] S. I. Bokarev, O. S. Bokareva, and O. Kühn, Coord. Chem. Rev. (2015), doi:10.1016/j.ccr.2014.12.016.
- [24] H. Iikura, T. Tsuneda, T. Yanai, and K. Hirao, J. Chem. Phys. **115**, 3540 (2001).
- [25] Y. Tawada, T. Tsuneda, S. Yanagisawa, T. Yanai, and K. Hirao, J. Chem. Phys. **120**, 8425 (2004).
- [26] M. Chiba, T. Tsuneda, and K. Hirao, J. Chem. Phys. **124**, 144106 (2006).
- [27] T. Yanai, D. P. Tew, and N. C. Handy, Chem. Phys. Lett. **393**, 51 (2004).
- [28] O. Bokareva, S. Bokarev, and O. Kühn, Phys. Chem. Chem. Phys. **14**, 4977 (2012).
- [29] J. S. Sears, T. Koerzdoerfer, C.-R. Zhang, and J.-L. Brédas, J. Chem. Phys. **135**, 151103 (2011).
- [30] T. Körzdörfer, J. S. Sears, C. Sutton, and J.-L. Brédas, J. Chem. Phys. **135**, 204107 (2011).
- [31] A. Karolewski, L. Kronik, and S. Kümmel, J. Chem. Phys. **138**, 204115 (2013).
- [32] S. Refaely-Abramson, R. Baer, and L. Kronik, Phys. Rev. B **84**, 075144 (2011).
- [33] E. Livshits and R. Baer, Phys. Chem. Chem. Phys. **9**, 2932 (2007).
- [34] T. Stein, L. Kronik, and R. Baer, J. Amer. Chem. Soc. **131**, 2818 (2009), ISSN 1520-5126.
- [35] T. Stein, L. Kronik, and R. Baer, J. Chem. Phys. **131**, 244119 (2009).
- [36] O. S. Bokareva, G. Grell, S. I. Bokarev, and O. Kühn, J. Chem. Phys. **in prep.** (2014).
- [37] K. King and R. Watts, J. Amer. Chem. Soc. **109**, 1589 (1987).
- [38] M. Yang, K. A. Jackson, and J. Jellinek, J. Chem. Phys. **125**, 144308 (2006).
- [39] K. Baishya, J. C. Idrobo, S. Ögüt, M. Yang, K. Jackson, and J. Jellinek, Phys. Rev. B **78**, 075439 (2008).
- [40] C. M. Aikens, S. Li, and G. C. Schatz, J. Phys. Chem. C **112**, 11272 (2008).
- [41] L. Zhao, L. Jensen, and G. Schatz, Nano Lett. **6**, 1229 (2006).
- [42] X.-F. Lang, P.-G. Yin, T.-T. You, L. Jiang, and L. Guo, ChemPhysChem **12**, 2468 (2011).
- [43] S. Boys and F. Bernardi, Mol. Phys. **19**, 553 (1970).
- [44] S. Simon, M. Duran, and J. J. Dannenberg, J. Chem. Phys. **105**, 472902 (1996).
- [45] M. J. Frisch, G. W. Trucks, H. B. Schlegel, G. E. Scuseria, M. A. Robb, J. R. Cheeseman, G. Scalmani, V. Barone, B. Mennucci, G. A. Petersson, et al., *Gaussian 09 Revision C.01*, Gaussian Inc. Wallingford CT 2009.
- [46] S. Bokarev, D. Hollmann, A. Pazidis, A. Neubauer, J. Radnik, O. Kühn, S. Lochbrunner, H. Junge, M. Beller, and A. Brückner, Phys. Chem. Chem. Phys. **16**, 4789 (2014).
- [47] J.-W. Song, T. Hirokawa, T. Tsuneda, and K. Hirao, J. Chem. Phys. **126**, 154105 (2007).
- [48] T. Stein, H. Eisenberg, L. Kronik, and R. Baer, Phys. Rev. Lett. **105**, 266802 (2010).
- [49] A. Karolewski, T. Stein, R. Baer, and S. Kümmel, J. Chem. Phys. **134**, 151101 (2011).
- [50] U. Salzner and A. Aydin, J. Chem. Theor. Comp. pp. 2568–2583 (2011).
- [51] T. Minami, S. Ito, and M. Nakano, Int. J. Quant. Chem. **113**, 252 (2013).
- [52] E. M. Fernández, J. M. Soler, I. L. Garzón, and L. C. Balbás, Phys. Rev. B **70**, 165403 (2004).
- [53] O. S. Bokareva and O. Kühn, Chem. Phys. **435**, 40 (2014).
- [54] S. Thomas, S. K. Nair, E. M. A. Jamal, S. H. Al-Harthi, M. R. Varma, and M. R. Anantharaman, Nanotechnology **19**, 075710 (2008).
- [55] Y. Ma, J. Lin, L. Zhu, H. Wei, D. Li, and S. Qin, Appl. Phys. A **102**, 521 (2011).
- [56] Y. Badr, M. A. E. Wahed, and M. Mahmoud, Appl. Surf. Sci. **253**, 2502 (2006).
- [57] P. Peng, A. Hu, and Y. Zhou, Appl. Phys. A **108**, 685 (2012).
- [58] V. N. Popok, I. Barke, E. E. Campbell, and K.-H. Meiwes-Broer, Surf. Sci. Rep. **66**, 347 (2011).
- [59] A. Hilger, M. Tenfelde, and U. Kreibitz, Appl. Phys. B **73**, 361 (2001).